https://doi.org/10.1016/j.vacuum.2020.109280 This is the Pre-Published Version.

Exchange bias effect in epitaxial $La_{0.35}Sr_{0.65}MnO_3/La_{0.7}Sr_{0.3}MnO_3$ bilayers: Impact of antiferromagnet growth conditions

Xuwen ZHAO, Hon Fai WONG, Yu Kuai LIU, Sheung Mei NG, Wang Fai CHENG, Chee Leung MAK and Chi Wah LEUNG*

Department of Applied Physics, The Hong Kong Polytechnic University, Hung Hom, Hong Kong, China

Abstract

Antiferromagnets have shown great potential for replacing ferromagnets in spintronic applications in recent years. In this work, antiferromagnetic $La_{0.35}Sr_{0.65}MnO_3$ (AFM-LSMO) thin films were grown on ultrathin ferromagnetic $La_{0.7}Sr_{0.3}MnO_3$ (FM-LSMO) layer over a wide temperature range. The different AFM-LSMO growth temperatures introduced variation of strain states in AFM-LSMO layer, changing the AFM-LSMO magnetic properties. Considering the model of thermally activated switching of antiferromagnetic grains, the measurement temperature and AFM-LSMO growth temperature-dependent exchange bias field and coercivity are explained. This work demonstrates the modulation of exchange bias effect in the FM-LSMO through the control of AFM-LSMO growth conditions, suggests possibility to control and probe oxide antiferromagnets via exchange bias coupling.

***Keywords**: pulsed laser deposition, perovskite oxide thin films, exchange bias effect*

*Corresponding author. Email address: dennis.leung@polyu.edu.hk (C.W. LEUNG)

© 2020. This manuscript version is made available under the CC-BY-NC-ND 4.0 license https://creativecommons.org/licenses/by-nc-nd/4.0/.

1. Introduction

Exchange bias effect, manifesting itself by the shifting of magnetic hysteresis loop and a significant coercivity enhancement, has been extensively studied due to their practical applications for sensors and related fundamental interfacial phenomena [1-3]. Various mechanisms based on domain interactions [4-6], interfacial super-exchange coupling [7], spin rearrangement at the antiferromagnet (AFM)/ferromagnet (FM) interface [8, 9], have been proposed to explain the phenomenon.

Until now, most of the studies on exchange bias effect are based on polycrystalline metal alloys or metal oxides as pinning layer [10]. It was until recently that the importance of material crystallinity on exchange bias effect has been recognized [11, 12]. In order to obtain a complete understanding of this interfacial phenomenon, high-quality AFM/FM materials with well-defined atomic interfaces are needed.

Recent technical advances in oxide thin film deposition and characterization have permitted precise control of complex oxide heterostructures with atomic level precision [13]. Among them, perovskite oxide multilayers have opened the possibility of investigating collective phenomena such as interfacial superconductivity [14], interfacial ferromagnetism [9, 15], due to the strong correlation between spin, charge, orbital and lattice degrees of freedom at the interface. Indeed, exchange bias effect was

observed not only in traditional AFM/FM structures but also in FM/FM [16], FM/paramagnet (PM) [17], and AFM/PM [9] structures.

To elucidate the impact of AFM/FM interface on exchange bias effect, ideally one should have a good control on the perovskite oxide heterostructures with atomically precise interfaces. Normally, metallic $La_{0.7}Sr_{0.3}MnO_3$ is used as the ferromagnetic layer since it has a relative high Currie temperature ($T_C \approx 370$K) [18]. However, magnetic properties of antiferromagnetic (La,Sr)MnO_3 thin films were seldom reported, let alone using them as the pinning layer.

In this work, we aim to establish exchange bias effect at the interface of antiferromagnetic $La_{0.35}Sr_{0.65}MnO_3$ (AFM-LSMO)/ferromagnetic $La_{0.7}Sr_{0.3}MnO_3$ (FM-LSMO) heterostructures. The structural compatibility between AFM-LSMO and FM-LSMO allows the epitaxial growth of heterostructures with sharp interfaces. In order to further modulate the microstructural and magnetic properties of AFM-LSMO, which can be reflected via exchange bias effect, the AFM-LSMO growth temperature was varied [19, 20]. The study would offer a handle to modify the exchange bias effect, and sheds light on the magnetic properties of AFM-LSMO layer under different growth conditions.

2. Experimental details

AFM-LSMO/FM-LSMO heterostructures were grown on $SrTiO_3$ (001) (STO) single-crystal substrates by pulsed laser deposition. Before deposition, the substrates

were pretreated to form step-like terraces with TiO_2 termination, details of which were reported previously [21]. In order to study the impact of AFM-LSMO growth conditions on the exchange bias effect, FM-LSMO (7 nm) layers were first deposited with standardized condition of 0.2 mbar O_2 ambient at a substrate temperature of 700 °C. After 5-minute post-annealing of FM-LSMO with O_2 at 13.3 mbar, the substrate temperature was adjusted to between 500 °C and 700 °C at the same oxygen ambient. Then AFM-LSMO layers were deposited at the new temperatures in 0.2 mbar O_2 pressure, followed by another 5-minute post-annealing with 13.3 mbar O_2 pressure before naturally cooled to room temperature in the same oxygen ambient. The targets were ablated by a KrF excimer laser (248 nm) with pulse energy of 220 mJ and at repetition rates of 1 Hz (for FM-LSMO) and 2 Hz (for AFM-LSMO), respectively. The microstructure of the samples was characterized by high-resolution x-ray diffraction (XRD, Smartlab, Rigaku). Surface morphology was characterized in air by atomic force microscopy (Bruker NanoScope 8) with tapping mode. Magnetic properties of the samples were studied by vibrating sample magnetometry (VSM, Quantum Design).

3. Results and discussion

Fig. 1(a) shows the XRD θ/2θ scan profile of AFM-LSMO (20 nm)/FM-LSMO (7 nm)/STO (001) structures with different AFM-LSMO growth temperatures. Clear (002) AFM-LSMO peaks and thickness fringes indicate good crystallinity and c-axis orientation of the layer. The diffraction peak of the thin FM-LSMO layer, on the other hand, overlaps with that of the substrate and AFM-LSMO. In-plane ϕ-scans (**Fig. 1(b)**)

were carried out to understand the epitaxy arrangement of AFM-LSMO/FM-LSMO on STO. All the ϕ-scan peaks taken on the (220) reflection exhibit four-fold symmetry with 90^0 intervals, and appear at the same azimuth angles, suggesting cube-on-cube growth of AFM-LSMO on STO. Note that ϕ-scan peaks of FM-LSMO were not shown here due to that in-plane (220) peak of thin FM-LSMO overlaps with that of STO. Considering coherent growth of AFM-LSMO and FM-LSMO layers on STO substrates, the shortening of *c*-axis of FM-LSMO (3.863 Å) and AFM-LSMO (3.797 to 3.815 Å), as compared to bulk FM-LSMO (3.889 Å) and AFM-LSMO (3.86 Å**)** [22, 23] values, suggests that both layers possess in-plane tensile stress.

From **Fig. 2** it is noticed that the (002) peak of AFM-LSMO shifts to higher angles with increasing growth temperature, which means the contraction of c-axis. Hence the antiferromagnetic growth temperature has a great impact on the AFM-LSMO microstructure, which in turn affects the bulk magnetic properties of AFM-LSMO. The extracted out-of-plane lattice constant of AFM-LSMO is plotted in **Fig. 2**. The key parameter dominating the physical properties of perovskite manganites is the *3d* orbital configuration of Mn ions. Strong Coulomb interactions between charged electrons and oxygen anions within the MnO_6 octahedral lead to lifted e_g orbitals with double degeneracy. Tensile strain suppresses the Coulomb interaction due to longer interaction length, shifting x^2-y^2 orbital to lower energy and attracting more electrons to occupy it. AFM-LSMO is an A-type antiferromagnet [24-28], meaning that ferromagnetic coupling among Mn ions occur in the in-plane direction and antiferromagnetic coupling

in the out-of-plane direction. The decreased c-axis length with rising growth temperature suggests larger in-plane tensile strain of AFM layer, which promotes the A-type antiferromagnetic ordering temperature [24].

The surface morphology of bilayer thin films was studied by *ex-situ* atomic force microscope. Fig. 2(b)-(f) present the surface morphologies of AFM-LSMO at different growth temperatures from 500 °C to 700 °C. Atomic terraces on substrates indicate a layer-by-layer growth of films. The root mean square roughness in all samples are less than 0.4 nm (Fig.2(g)), showing the good surface morphology of films.

With AFM-LSMO growth temperature between 550 °C and 700 °C, the full-width at half-maximum (FWHM) of the rocking curves for (002) peaks of AFM-LSMO is around 0.1º, suggesting low mosaic spread. For AFM-LSMO layer grown at 500 °C, although the FWHM of rocking curve is also 0.1°, it shows a clear two-peak configuration with a sharp peak superimposed on a broad peak compared with that grown at 600 °C (see in Fig. 3), which implies the presence of a layer of different mosaic spread, possibly a partial relaxed layer [29].

Temperature-dependent magnetic hysteresis loops (*M-H* loops) were obtained from the samples by field-cooling from 350 K to 10 K in an external magnetic field of 1T, with all loops measured with increasing sample temperatures to suppress possible memory effect [30]. Note that 10 training cycles were conducted before the actual *M-H* loops were extracted to eliminate the training effect [31]. **Fig. 4(a)** displays the *M-H* loops of

AFM-LSMO/FM-LSMO samples with different AFM-LSMO growth temperatures; the *M-H* loop of a plain FM-LSMO layer at 10 K is also displayed. Significant shift of *M-H* loops and coercivity enhancement are observed in most samples. For future analysis, the exchange bias field (H_{EB}) and coercive field (H_C) for the samples at 10 K were extracted (**Fig. 4(b)). T**he largest H_{EB} and H_C were found in the sample with AFM-LSMO deposited at around 600 °C. This can be ascribed to the competition between interfacial imperfection and crystallinity in the bulk of AFM layer. Usually, exchange bias effect is ascribed to the interfacial effect. And from the surface morphology in Fig. 2(g), we can see that the roughness is a little higher at 600 °C and 650 °C. On the other hand, previous reports showed the impact of the antiferromagnet bulk on exchange bias [20. In this work, the antiferromagnetic growth temperatures not only could change the interface but also change the bulk as XRD results (Fig. 1(a)) indicated.

The temperature dependences of H_{EB} and H_C with different AFM-LSMO growth temperatures are shown in **Fig. 4(c)** and **4(d)**, respectively. According to previous reports [24, 32, 33], both single crystal and AFM-LSMO thin film (30 nm) should be magnetically ordered around 240 ~ 260 K. Our results indicate that exchange bias disappears (i.e. T_B) at around 150 K, which is much less than the Néel temperature (T_N) of AFM-LSMO (~ 250 K) [32, 33]. Moreover, the exponential decay of H_{EB} and H_C with temperature are usually ascribed to the existence of frustration due to competing interactions, suggesting a common mechanism for the exchange bias and coercivity as reported in $La_{2/3}Ca_{1/3}MnO_3/La_{1/3}Ca_{2/3}MnO_3$ bilayers and superlattices [6, 34-36]. The

temperature dependence of H_{EB} and H_C can be fitted by the phenomenological equations [6]:

$$H_{EB}(\mathrm{T}) = H_{EB}^{0}\mathrm{e}^{(-\mathrm{T}/T_1)} \quad (1)$$

$$H_{C}(\mathrm{T}) = H_{C}^{0}\mathrm{e}^{(-\mathrm{T}/T_2)} \quad (2)$$

where H_{EB}^{0} and H_C^{0} are H_{EB} and H_C extrapolated to zero temperature, T_1 and T_2 are the energy barrier for thermal activation of the magnetic interface response for the exchange bias effect.

The agreement between experimental data and fitting results, as well as the observation that T_B is far below the magnetic ordering temperature of AFM-LSMO (T_N) and FM-LSMO (T_C), can be understood by the thermally-activated switching of AFM grains [5, 6, 34, 37, 38]. In this model, the AFM domains are confined within individual crystals, the temperature dependence of exchange bias effect arises from thermally-activated switching of AFM grains and the AFM domain wall energy in the grains. There are two main factors which decide the temperature dependence of the exchange bias behavior: the saturation behavior of unidirectional anisotropy at low temperatures, and the thermal stability of the AFM grains. According to prediction of the model, once the interfacial coupling energy (J_{int}) is larger than the domain wall energy (σ) in AFM grains, H_{EB} continue to increase with lowering temperature. As shown in **Fig. 4(c)**, temperature dependent curves with different AFM growth

temperatures show a non-saturated exchange bias field at low temperatures, suggesting that the J_{int} of AFM-LSMO/FM-LSMO is larger than the σ.

On the other hand, the ratio (*b*) between σ (times the area of the grain) and the thermal energy can be used to characterize thermal stability of the AFM grains. For samples with different AFM-LSMO growth temperatures, *b* is small at temperatures just below T_N and AFM grains are stabilized slowly. Hence, until only when the temperature is far below T_N, the AFM grains can contribute to unidirectional anisotropy. This could explain why T_B is below T_N in all samples. Moreover, T_B is found to *decrease* with increasing AFM-LSMO growth temperature (inset of **Fig. 4(c)**), which is contrary to our expectation. As mentioned before, increasing AFM-LSMO growth temperature is beneficial for promoting AFM crystallinity and hence spin ordering [38]. Based on $\sigma \propto \sqrt{A_{AF}K_{AF}}$, and the approximations that the antiferromagnetic moment $m_{AF} \propto (T_N - T)^{1/3}$ (T represents the measurement temperature), the uniaxial anisotropy constant $K_{AF} \propto m_{AF}^3$, and the exchange stiffness constant $A_{AF} \propto m_{AF}^2$, we assume that $b \propto (T_N - T)^{5/6}/T_N$ [38]. With rising AFM growth temperature, *b* should increase due to higher spin ordering temperature, which is contrast to our observation. More detailed experiments need to be conducted to verify the interfacial microstructure effect on the exchange bias effect in manganite multilayers.

4. Conclusion

In summary, high-quality AFM-LSMO/FM-LSMO epitaxial heterostructures were grown on TiO_2-terminated $SrTiO_3$ (001) substrates by pulsed laser deposition. X-ray diffraction suggested antiferromagnetic growth temperature can modify the strain state of AFM-LSMO layer, influencing the magnetic properties of heterostructures. Exchange bias effect, together with enhanced coercivity were observed in these structures. Temperature-dependent exchange bias field and coercivity can be understood by thermally activated switching of antiferromagnetic grains, shedding insights on the physical mechanism at the interface of AFM-LSMO/FM-LSMO heterostructures.

Acknowledgements

This work was supported by the Hong Kong Research Grant Council (PolyU 153027/17P), and the Hong Kong Polytechnic University (1-ZVGH, G-UAGJ).

References

[1] W.H. Meiklejohn, C.P. Bean, New magnetic anisotropy, Phys. Rev. 105 (1957) 904-913.

[2] F. Hellman, A. Hoffmann, Y. Tserkovnyak, G.S.D. Beach, E.E. Fullerton, C. Leighton, A.H. MacDonald, D.C. Ralph, D.A. Arena, H.A. Dürr, P. Fischer, J. Grollier, J.P. Heremans, T. Jungwirth, A.V. Kimel, B. Koopmans, I.N. Krivorotov, S.J. May, A.K. Petford-Long, J.M. Rondinelli, N. Samarth, I.K. Schuller, A.N. Slavin, M.D. Stiles, O. Tchernyshyov, A. Thiaville, B.L. Zink, Interface-induced phenomena in magnetism, Rev. Mod. Phys. 89 (2017) 025006.

[3] H.Y. Hwang, Y. Iwasa, M. Kawasaki, B. Keimer, N. Nagaosa, Y. Tokura, Emergent phenomena at oxide interfaces, Nat. Mater. 11 (2012) 103-113.

[4] K.D.U. U. Nowak, J. Keller, P. Milte´nyi, B. Beschoten, and G. Gu¨ntherodt, Domain state model for exchange bias. I. Theory, Phys. Rev. B 66 (2002) 014430.

[5] P.M.n. J. Keller, B. Beschoten, G. Gu¨ntherodt, U. Nowak and K. D. Usadel, Domain state model for exchange bias. II. Experiments, Phys. Rev. B 66 (2002) 014431.

[6] N. Moutis, C. Christides, I. Panagiotopoulos, D. Niarchos, Exchange-coupling properties of $La_{1-x}Ca_xMnO_3$ ferromagnetic/antiferromagnetic multilayers, Phys. Rev. B 64 (2001) 094429.

[7] P. Yu, J.S. Lee, S. Okamoto, M.D. Rossell, M. Huijben, C.H. Yang, Q. He, J.X. Zhang, S.Y. Yang, M.J. Lee, Q.M. Ramasse, R. Erni, Y.H. Chu, D.A. Arena, C.C. Kao, L.W. Martin, R. Ramesh, Interface ferromagnetism and orbital reconstruction in $BiFeO_3$-$La_{0.7}Sr_{0.3}MnO_3$ heterostructures, Phys. Rev. Lett. 105 (2010) 027201.

[8] A.Y. Borisevich, H.J. Chang, M. Huijben, M.P. Oxley, S. Okamoto, M.K. Niranjan, J.D. Burton, E.Y. Tsymbal, Y.H. Chu, P. Yu, R. Ramesh, S.V. Kalinin, S.J. Pennycook, Suppression of octahedral tilts and associated changes in electronic properties at epitaxial oxide heterostructure interfaces, Phys. Rev. Lett. 105 (2010) 087204.

[9] C. He, A.J. Grutter, M. Gu, N.D. Browning, Y. Takamura, B.J. Kirby, J.A. Borchers, J.W. Kim, M.R. Fitzsimmons, X. Zhai, V.V. Mehta, F.J. Wong, Y. Suzuki, Interfacial ferromagnetism and exchange bias in $CaRuO_3/CaMnO_3$ superlattices, Phys. Rev. Lett. 109 (2012) 197202.

[10] J. Nogue´, I.K. Schuller, Exchange bias, J. Mang. Mang. Mater. 192 (1999) 203-232.

[11] A.K. Suszka, O. Idigoras, E. Nikulina, A. Chuvilin, A. Berger, Crystallography-driven positive exchange bias in Co/CoO bilayers, Phys. Rev. Lett. 109 (2012) 177205.

[12] E. Młyńczak, B. Matlak, A. Kozioł-Rachwał, J. Gurgul, N. Spiridis, J. Korecki, Fe/CoO(001) and Fe/CoO(111) bilayers: Effect of crystal orientation on the exchange bias, Phys. Rev. B 88 (2013) 085442.

[13] E. Dagotto, When oxides meet face to face, Science 318 (2007) 1076-1077.

[14] N. Reyren, S. Thiel, A.D. Caviglia, L.F. Kourkoutis, G. Hammerl, C. Richter, C.W. Schneider, T. Kopp, A.-S. Rüetschi, D. Jaccard, M. Gabay, D.A. Muller, J.-M. Triscone, J. Mannhart, Superconducting interfaces between insulating oxides, Science 317 (2007) 1196-1199.

[15] Z. Chen, Z. Chen, Z.Q. Liu, M.E. Holtz, C.J. Li, X.R. Wang, W.M. Lu, M. Motapothula, L.S. Fan, J.A. Turcaud, L.R. Dedon, C. Frederick, R.J. Xu, R. Gao, A.T.

N'Diaye, E. Arenholz, J.A. Mundy, T. Venkatesan, D.A. Muller, L.W. Wang, J. Liu, L.W. Martin, Electron accumulation and emergent magnetism in $LaMnO_3/SrTiO_3$ heterostructures, Phys. Rev. Lett. 119 (2017) 156801.

[16] M. Ziese, I. Vrejoiu, E. Pippel, P. Esquinazi, D. Hesse, C. Etz, J. Henk, A. Ernst, I.V. Maznichenko, W. Hergert, I. Mertig, Tailoring magnetic interlayer coupling in $La_{0.7}Sr_{0.3}MnO_3/SrRuO_3$ superlattices, Phys. Rev. Lett. 104 (2010) 167203.

[17] M. Gibert, P. Zubko, R. Scherwitzl, J. Iniguez, J.M. Triscone, Exchange bias in $LaNiO_3$-$LaMnO_3$ superlattices, Nat. Mater. 11 (2012) 195-198.

[18] H.Y. Hwang, S.W. Cheong, P.G. Radaelli, M. Marezio, B. Batlogg, Lattice effects on the magnetoresistance in doped $LaMnO_3$, Phys. Rev. Lett. 75 (1995) 914-917.

[19] P.J.v.d. Zaag, Y. Ijiri, J.A. Borchers, L.F. Feiner, R.M. Wolf, J.M. Gaines, R.W. Erwin, M.A. Verheijen, Difference between blocking and Néel temperatures in the exchange biased Fe_3O_4/CoO system, Phys. Rev. Lett. 84 (2000) 6102-6105.

[20] P. Miltényi, M. Gierlings, J. Keller, B. Beschoten, G. Güntherodt, Diluted antiferromagnets in exchange bias: proof of the domain state model, Phys. Rev. Lett. 84 (2000) 4224-4227.

[21] H.F. Wong, S.M. Ng, W.F. Cheng, Y. Liu, X. Chen, D. von Nordheim, C.L. Mak, J. Dai, B. Ploss, C.W. Leung, Enhanced tunability of electrical and magnetic properties in

(La,Sr)MnO_3 thin films via field-assisted oxygen vacancy modulation, Solid-State Electronics 138 (2017) 56-61.

[22] M. Huijben, L.W. Martin, Y.-H. Chu, M.B. Holcomb, P. Yu, G. Rijnders, D.H.A. Blank, R. Ramesh, Critical thickness and orbital ordering in ultrathin $La_{0.7}Sr_{0.3}MnO_3$ films, Phys. Rev. B 78 (2008) 094413.

[23] https://www.promes.cnrs.fr/uploads/pdfs/production/rapport_2016/SASI_vens.pdf.

[24] S.J. May, P.J. Ryan, J.L. Robertson, J.W. Kim, T.S. Santos, E. Karapetrova, J.L. Zarestky, X. Zhai, S.G. te Velthuis, J.N. Eckstein, S.D. Bader, A. Bhattacharya, Enhanced ordering temperatures in antiferromagnetic manganite superlattices, Nat. Mater. 8 (2009) 892-897.

[25] A.T. Wong, C. Beekman, H. Guo, W. Siemons, Z. Gai, E. Arenholz, Y. Takamura, T.Z. Ward, Strain driven anisotropic magnetoresistance in antiferromagnetic $La_{0.4}Sr_{0.6}MnO_3$, Appl. Phys. Lett. 105 (2014) 052401.

[26] Y. Tokura, N. Nagaosa, Orbital physics in transition-metal oxides, Science 288 (2000) 462-467.

[27] Y. Konishi, Z. Fang, M. Izumi, T. Manako, M. Kasai, H. Kuwahara, M. Kawasaki, K. Terakura, Y. Tokura, Orbital-state-mediated phase-control of manganites, J. Phys. Soc. Jan. 68 (1999) 3790-3793.

[28] Z. Fang, I.V. Solovyev, K. Terakura, Phase diagram of tetragonal manganites, Phys. Rev. Lett. 84 (2000) 3169-3172.

[29] S. Jin, G. Gao, W. Wu, X. Zhou, Effect of angular-distortion-induced strain on structural and transport properties of epitaxial $La_{0.7}Sr_{0.3}MnO_3$ thin films, J. Phys. D: Appl. Phys. 40 (2007) 305-309.

[30] C.W. Leung, M.G. Blamire, Interaction between ferromagnetic/antiferromagnetic systems across a common antiferromagnetic spacer, J. Appl. Phys. 94 (2003) 7373-7375.

[31] C.W. Leung, M.G. Blamire, Interaction between exchange-bias systems in$Ni_{80}Fe_{20}$/$Fe_{50}Mn_{50}$/Cotrilayers, Phys. Rev. B 72 (2005) 054429.

[32] J. Hemberger, A. Krimmel, T. Kurz, H.A. Krug von Nidda, V.Y. Ivanov, A.A. Mukhin, A.M. Balbashov, A. Loidl, Structural, magnetic, and electrical properties of single-crystalline $La_{1-x}Sr_xMnO_3$ ($0.4 < x < 0.85$), Phys. Rev. B 66 (2002).

[33] Y. Moritomo, T. Akimoto, A. Nakamura, K. Ohoyama, M. Ohashi, Antiferromagnetic metallic state in the heavily doped region of perovskite manganites, Phys. Rev. B 58 (1998) 5544-5549.

[34] C.C. I. Panagiotopoulos, M. Pissas and D. Niarchos, Exchange-biasing mechanism in $La_{2/3}Ca_{1/3}MnO_3$/$La_{1/3}Ca_{2/3}MnO_3$ multilayers, Phys. Rev. B 60 (1999) 485-491.

[35] P. Prieto, M.E. Gomez, G. Campillo, A. Berger, E. Baca, R. Escudero, F. Morales, J. Guimpel, N. Haberkorn, Exchange-coupling effect and magnetotransport properties in epitaxial $La_{2/3}Ca_{1/3}MnO_3/La_{1/3}Ca_{2/3}MnO_3$ superlattices, Phys. Status Solidi A 201 (2004) 2343-2346.

[36] E. Restrepo-Parra, J.D. Agudelo, J. Restrepo, Exchange bias in (La,Ca)MnO_3 bilayers: influence of cooling process, Model. Simul. Mater. SC 20 (2012) 085009.

[37] K.D.U. U. Nowak, J. Keller, P. Milte´nyi, B. Beschoten, and G. Gu¨ntherodt, Domain state model for exchange bias. I. Theory, Phys. Rev. B 66 (2002) 014430.

[38] M.D. Stiles, R.D. McMichae, Temperature dependence of exchange bias in polycrystalline ferromagnet-antiferromagnet bilayers, Phy Rev B 60 (1999) 12950-12956.

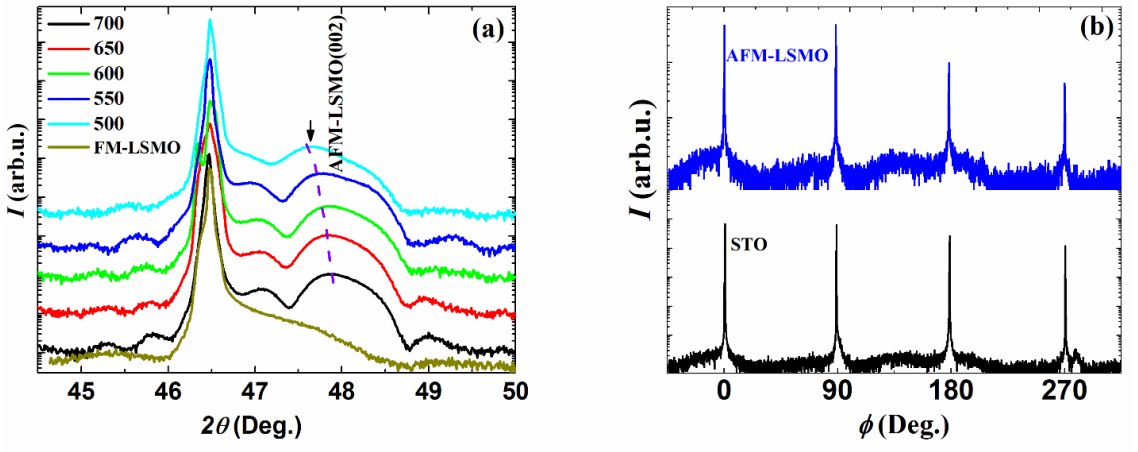

Fig. 1. Structure characterization of AFM-LSMO/FM-LSMO/STO (001) structures. (a) Out-of-plane θ/2θ profile; legends show AFM-LSMO growth temperatures in °C. (b) ϕ-scan patterns of AFM-LSMO/FM-LSMO/STO structure for AFM-LSMO growth temperature of 600 °C.

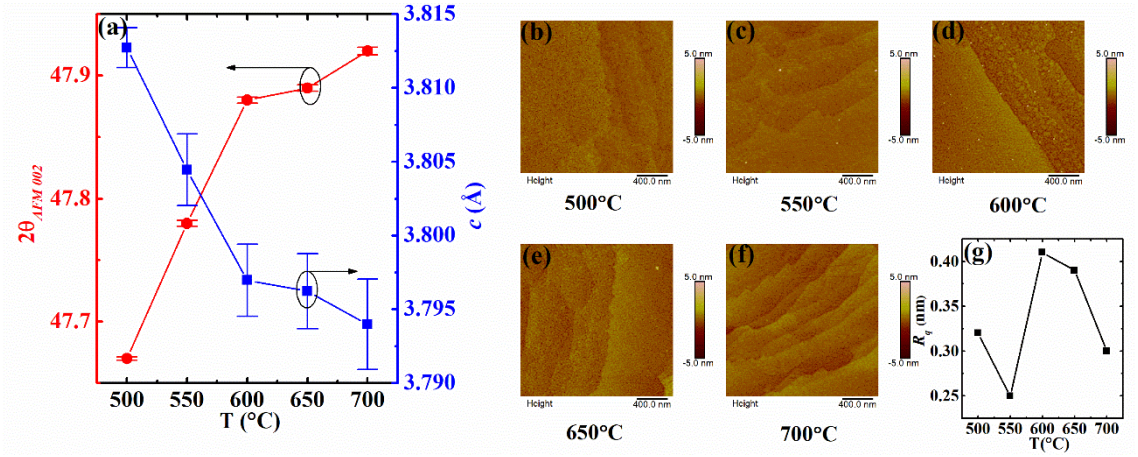

Fig. 2. (a) (002) peak positions (red circles) and out-of-plane lattice constants (blue squares) of AFM-LSMO as a function of growth temperatures. (b)-(f) Surface morphology of bilayers with AFM-LSMO growth temperature at 500ºC, 550ºC, 600ºC, 650ºC and 700ºC, respectively. Note that all images are 2×2 μm^2. (g) The root-mean square roughness of samples with different AFM-LSMO growth temperatures.

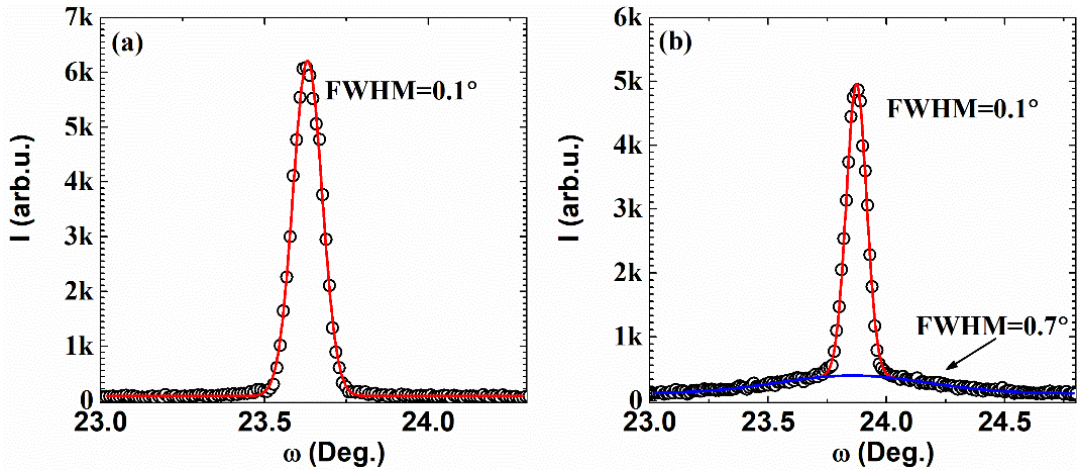

Fig. 3. Rocking curves of (002) peak of AFM-LSMO grown at different temperatures: (a) 600 °C, and (b) 500 °C. Red and blue lines are Gaussian fits of the curves.

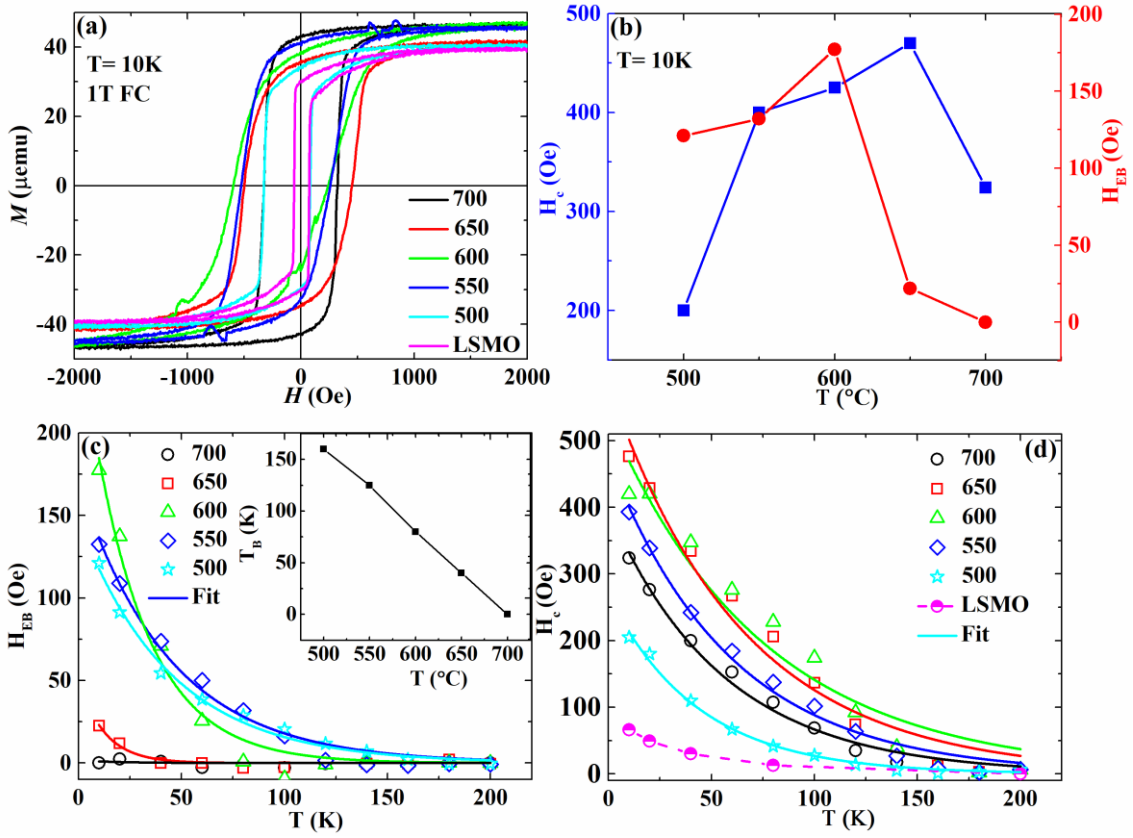

Fig. 4. Magnetic properties of AFM-LSMO/FM-LSMO/STO structures. (a) M-H loops at 10K after 1T field-cooling. (b) Coercivity (blue squares) and exchange bias field (red dots) as a function of AFM-LSMO growth temperatures. (c) Temperature dependence of exchange bias field of AFM-LSMO/FM-LSMO/STO with different AFM-LSMO growth temperatures. Inset: the blocking temperature as a function of AFM-LSMO growth temperatures. (d) Temperature dependence of coercivity of AFM-LSMO/FM-LSMO/STO with different AFM-LSMO growth temperatures. In (a), (c) and (d), legends show AFM-LSMO growth temperatures in °C.